Appl. Phys. A 77, 217–221 (2003)
DOI: 10.1007/s00339-003-2142-4

**Applied Physics A**
**Materials Science & Processing**

C. KEYSER[1,*]
G. SCHRIEVER[1,**]
M. RICHARDSON[1,✉]
E. TURCU[2]

# Studies of high-repetition-rate laser plasma EUV sources from droplet targets

[1] School of Optics & CREOL, University of Central Florida, Orlando, FL 32816, USA
[2] JMAR Research Inc. 3956 Sorrento Valley Blvd. San Diego, CA 92121, USA

**Received: 31 October 2002/Accepted: 8 February 2003**
**Published online: 28 May 2003 •** 

**ABSTRACT** The water droplet laser plasma source has been shown to have many attractive features as a continuous, almost debris-free source for extreme ultraviolet (EUV) and X-ray applications. Through a dual experimental and theoretical study, we analyze the interaction physics between the laser light and the target. The hydrodynamic laser plasma simulation code, Medusa103 is used to model the electron density distribution for comparison to electron density distributions obtained through Abel inversion of plasma interferograms. In addition, flat field EUV spectra are compared to synthetic spectra calculated with the atomic physics code RATION.

**PACS** 52.38.MF

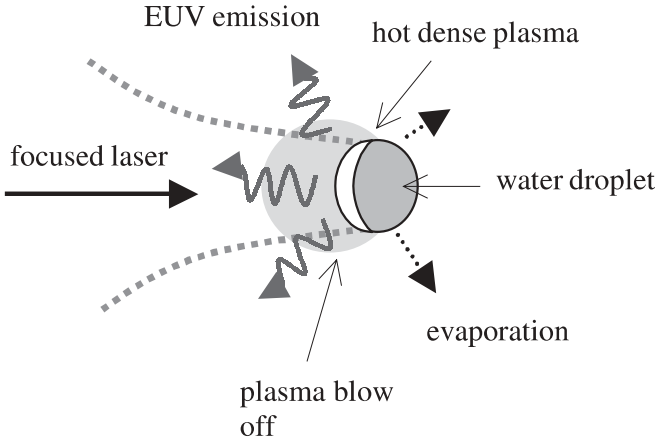


**FIGURE 1** Principle of the laser plasma droplet target

## 1 Introduction

The water droplet laser target has received considerable attention as a bright, clean soft X-ray point source to meet the advancing needs of technological applications such as lithography. The cryogenic water droplet target was first proposed as a debris-free mass-limited laser plasma target source of EUV line radiation in 1993 [1, 2]. As a mass limited target, the dimensions of the water droplet are closely matched to laser focal spot size to limit the ablated and shocked from mass from the target [3–5]. This is important because it has previously been shown that mass limited targets will be necessary for EUV lithography to minimize destructive debris produced from the plasma [6]. Other advantages to using a fluid target include the evaporation and subsequent evacuation of any material ejected from the target before it can reach nearby optics and the ease of delivery to the laser focal region [7].

Figure 1 illustrates the principle of the water droplet as a laser plasma point source. A high intensity laser pulse is focused onto a water droplet causing the formation of a hot dense plasma. The drops are produced by a jet capillary at frequencies of 20–200 kHz having diameters in the range of 30–80 μm. Past studies of the water droplet plasma have focused on the spectral emission and debris characterization. Spectra of the oxygen emission in the 10–18 nm region were recorded using a flat field spectrograph [8, 9]; the resulting spectrum is shown in Fig. 2 [10]. The presence of strong 13 nm line emission from the $4d$–$2p$ transition in Li like oxygen is seen in this spectrum. The shaded region represents the reflective mirror bandpass of the Mo/Si mirrors that are to be used in EUV lithography steppers. The spectrum indicates that there is complete overlap of the mirror bandpass and the oxygen 13 nm line. The maximum recorded conversion efficiency for the water droplet target was $0.63\%/4\pi$ sr [10]. Characterization of the water droplet plasma debris production was accomplished by monitoring the reflectivity of a Mo/Si mirror placed at 32 mm from the plasma as a function of the number of laser pulses. This was accomplished for the case of no debris interdiction technique and for the case of an ion repelling electric field created by placing the mirror housing at +100 V [10]. The results are shown in Fig. 3. The oscillations of the reflectivity are the result of alternating layers of Mo and Si being sputtered away. The shielding effect of the ion repeller field was ascertained by counting the number of Mo/Si layers that were sputtered away for each case. The application of the electric field increased the lifetime of the mirror by a factor of 7 as compared to the case with no repeller field.

To attain a more comprehensive understanding of the water droplet plasma expansion dynamics as well as spectral emission and debris ejection characteristics, theoretical sim-

✉ Fax: +1-407/823-3570, E-mail: mrichard@mail.ucf.edu
*Present address:* Naval Reseach Laboratory, Washington D.C.
**Present address:* Xtreme Technologies, Göttingen, Germany.

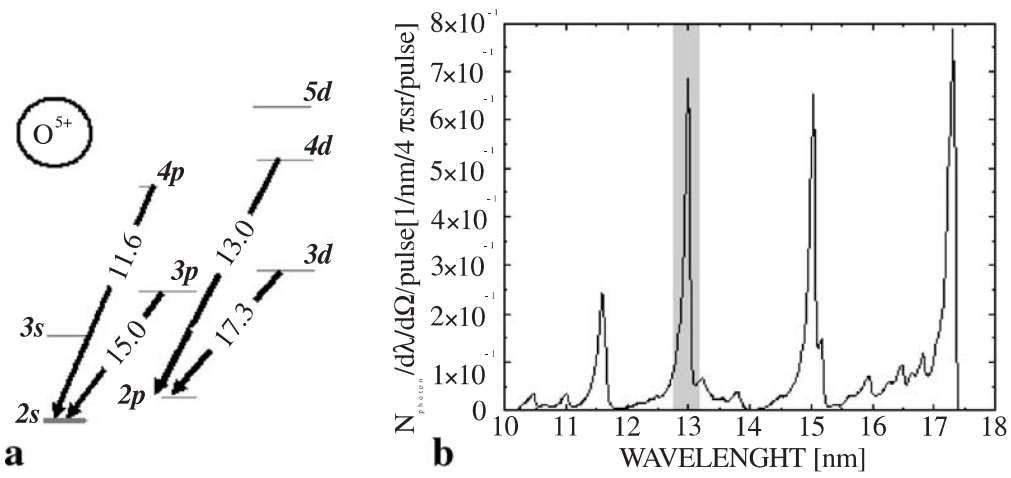


**FIGURE 2** **a** $O^{5+}$ spectra from Li like Oxygen **b** Energy level structure of $O^{5+}$

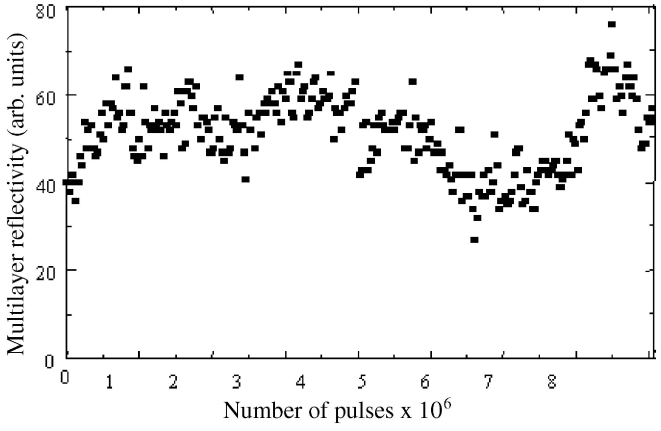


**FIGURE 3** Multilayer mirror reflectivity as a function of the number of laser pulses

ulations and optical diagnostics of the laser plasma are being made.

## 2 Theoretical simulations

Laser plasma simulations codes are useful in ascertaining information on the influence of various laser and target parameters on plasma heating and can therefore provide valuable insight into the wavelength and intensity dependence of the radiation emission from the plasma. MEDUSA 103 is a 1-D hydrodynamic simulation code that allows the user to specify the laser plasma interaction parameters: these parameters include the laser pulse length, intensity, wavelength and pulse shape as well as the target geometry and composition [11]. Based on these parameters and a number of physical switches that specify the interaction physics the code calculates the plasma density, electron and ion temperature, average ion charge state, and plasma velocity as a function of time and space. Figure 4 shows the simulation results for the plasma expansion and heating as a function of time relative to the peak of the laser pulse for our experimental conditions, which include the following: $I = 4 \times 10^{11}\,\mathrm{W/cm^2}$, pulse length $= 10$ ns, a laser spot size $= 80\,\mu$m, $\lambda = 1.064\,\mu$m, and a water droplet radius $= 20\,\mu$m.

Characteristic of nanosecond laser plasmas, most of the X-ray emission occurs near critical density where there exists a relatively high electron temperature and ion density. For a 1 μm ionizing laser pulse the critical density is $\sim 10^{21}\,\mathrm{cm^{-3}}$. Simulations with the synthetic spectral code RATION indicate that the optimum plasma temperature for populating the $4d$ level of $O^{5+}$ at critical density is about 28 eV [3, 4]. It is seen that at the peak of the laser pulse, at 0 ns, the temperature at critical density is about 30 eV. One can therefore expect strong 13 nm line emission from the water droplet target under these irradiation conditions.

The spectral simulation code RATION has been used to model the Li like oxygen emission from the water droplet plasma [12]. Given the atomic number of the plasma species, RATION calculates the radiation emission of H, He, and Li like ions as a function of electron density and plasma temperature. The spectrum produced by RATION is shown in Fig. 5. The synthetic spectrum is seen to be in good agreement with the experimental spectra recorded by the flat field spectrograph.

## 3 Optical diagnostics

Interferometry is a powerful optical probe technique capable of providing high resolution spatial and temporal information about an expanding plasma. We have employed the polarized light interferometer to study the water droplet plasma expansion dynamics [13, 14]. Figure 6 illustrates the simplicity of this device. The lens L images the object O, the plasma, into the image plane. The Wollaston prism creates two orthogonally polarized images that overlap in the image plane and are separated by an angle $\varepsilon$. Interference between these two images is accomplished by a pair of polarizers, $P_1$ and $P_2$, oriented either parallel or perpendicular to one another. In order to form high contrast fringes in the image plane, P2 is oriented such that the two originally orthogonal images will, after passing through $P_2$ , have the same polarization and intensity. The fringe separation in the object plane is given by $i = (\lambda f/b\varepsilon)$, where $\lambda$ is the wavelength, $f$ is the focal length of the imaging lens, $\varepsilon$ is the angle between the two deviated images, and $b$ is the distance between the Wollaston prism and the lens focal plane [14]. The fringe orientation can be changed by rotating the polarization

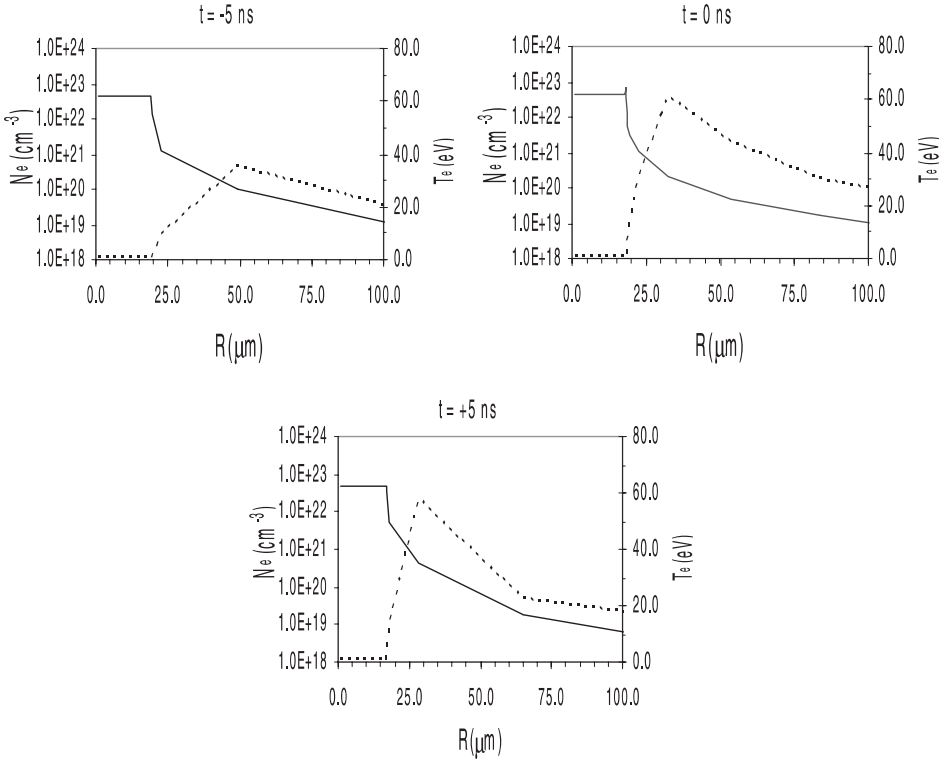


**FIGURE 4** MEDUSA simulations shown at times relative to the laser pulse peak

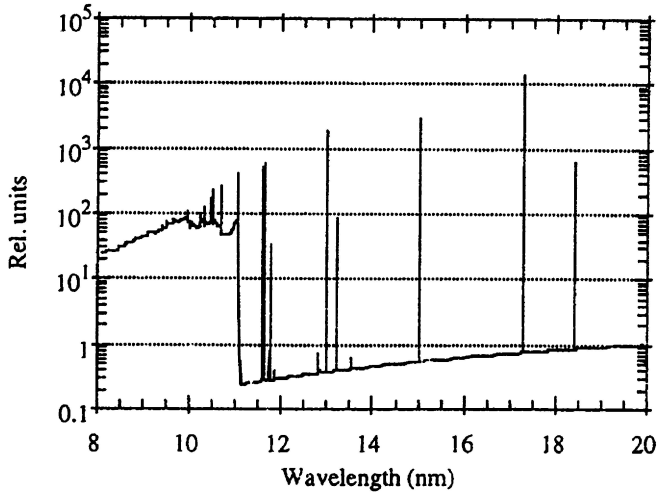


**FIGURE 5** RATION spectra calculated for the water droplet plasma

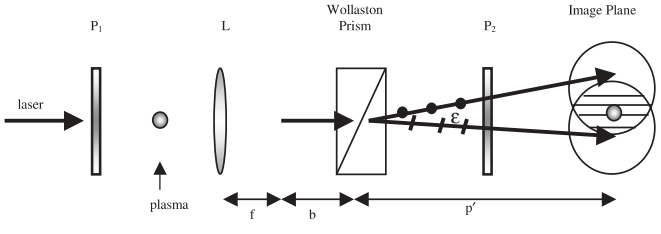


**FIGURE 6** Polarized light interferometer

elements and the fringe spacing is varied by changing the distance between the focal plane of the lens and the Wollaston prism, $b$. The Wollaston prism used in our experiments is composed of Quartz and has $\varepsilon = 8.7$ mrad. Using a 7.5 cm focal length lens and $b = 37.7$ cm the fringe spacing is calculated to be 12.1 μm.

The cumulative phase difference between light rays passing through equal lengths of plasma and vacuum is given by [15]

$$\Delta\phi = k_0 \int \left( \left( 1 - \frac{n_e}{n_c} \right)^{1/2} - 1 \right) \mathrm{d}l \approx \frac{k_0}{2n_c} \int n_e \, \mathrm{d}l \qquad (1)$$

where the plasma index of refraction is $N = (1 - n_e/n_c)^{1/2}$, $n_e$ is the electron density, and $n_c = m_e \varepsilon_o \omega^2 / 4\pi e^2$ is the critical density. In writing the expression on the right side it was assumed that $n_e \ll n_c$. In the event that the plasma is spherically or cylindrically symmetric one can extract the radial distribution of the electron distribution from the above chordal integral by applying the Abel inversion given by [15]

$$n_e(r) = \frac{n_c}{k_0} \frac{-1}{\pi} \int_r^R \frac{\mathrm{d}\Delta\phi}{\mathrm{d}y} \frac{1}{\sqrt{y^2 - r^2}} \mathrm{d}y \qquad (2)$$

Here $k_0$ is the probe wavenumber, $R$ is the plasma radius where $n_e = 0$, and $y$ is the coordinate transverse to the axis of symmetry and the line of sight. The code Interferometric Data Evaluation Algorithms (IDEA) was used to calculate the plasma induced phase shift and compute Abel inversion [16].

Figure 6 illustrates the experimental set up being used for the optical diagnostic experiments. The ionizing laser beam is produced by a Spectra Physics $Q$-switched Nd:YAG laser operating at 100 Hz, having 10 ns (FWHM), 270 mJ pulses that are focused to $4 \times 10^{11}$ W/cm$^2$ on target by a $f/2$ lens. Due to the rapid expansion rates of laser plasmas a short probe pulse is necessary to avoid fringe blurring in interferograms. The probe beam is initially formed by passing the Nd:YAG fundamental beam through a second harmonic generator (SHG) producing a 6 ns, 532 nm beam. Following the

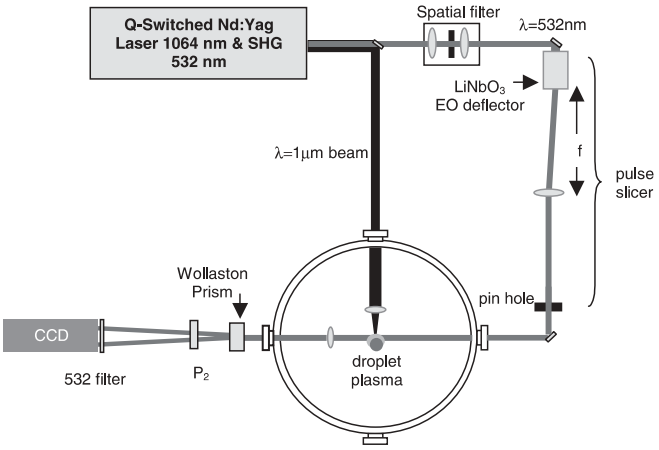


**FIGURE 7** Experimental set up for interferometry of the laser plasma

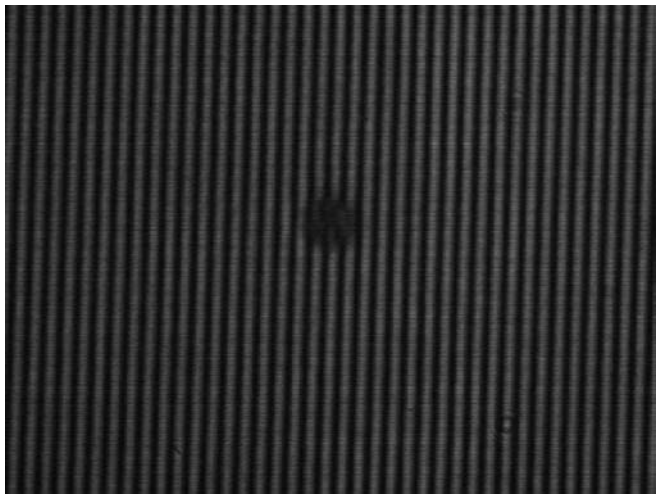

**FIGURE 8** Interferogram of a water droplet

SHG, the 532 nm beam is spatially filtered to remove beam non-uniformities. The probe pulse is further shortened to a duration of about 1 ns by the application of a pulse slicing technique [17]. A 5 kV, 10 ns rise time voltage pulse is applied to a $LiNbO_3$ crystal having a quadrupole electrode arrangement as the SHG pulse passes through. The high voltage pulse produces a time varying linear gradient in the crystal index of refraction causing an angular deflection of the pulse. By placing the exit face of the crystal in the focal plane of a 1 m focal length lens the deflected pulse is redirected parallel to the axis of the crystal. As this beam is swept across a 300 μm pin hole, a short 1 ns pulse is sliced out of the original 6 ns 532 nm pulse. The plasma was imaged by a $f/3$ lens with a magnification of 17.75 and a spatial resolution of about 5 μm.

Figures 8 and 9 are interferograms showing a $\sim 35$ μm diameter water droplet and the plasma at the peak of the 1 μm ionizing pulse, respectively; the laser is incident from the left side of the photo. The dark region in the center region of Fig. 9 is due to the opaqueness of the plasma above critical density ($n_c = 4 \times 10^{21}$ cm$^{-3}$ for the 532 nm probe) and strong refraction of the probe beam by a steep electron density gradient. The crescent shaped region of enhanced brightness to the left of the dark region is the result of this refractive affect, which inhibits probing to the critical density. The circle in the center of the plasma indicates the approximate dimensions and position of the 35 μm drop before irradiation. The circular shaped fringes in the region of direct laser droplet interaction, reveal, to first order, spherical symmetry in the expanding plasma. In the region above the drop, a plasma wake is apparent. On the rear side of the plasma there are at least two plasma jets as evidenced by a line of ripples in the fringe pattern. In the area directly behind the plasma, very small fringe shifts indicate the presence of a low density plasma. Superimposed on this quasi-uniform density pattern are perturbations in the interferogram indicating the presence of a non-uniform field of either water vapor or plasma leakage.

Figure 10 is a plot of the Abel inverted electron density distribution along the axis of the incident laser beam. Also shown in the plot is an exponential fit to the data; the fit is extremely good indicating an exponential plasma blow off in the under-dense region of the plasma. The contour map in Fig. 11 displays the two dimensional results of the Abel inversion. The cross hatched region in the center of the contour plot represents the opaque area of the plasma; the circle in

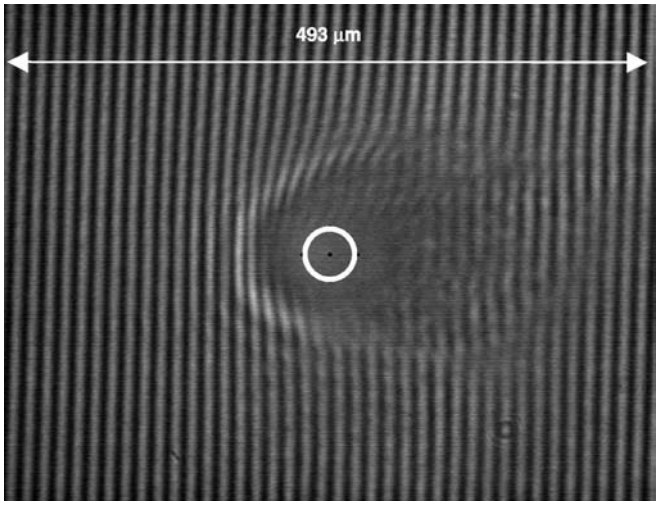


**FIGURE 9** Interferogram of droplet plasma at peak of ionizing pulse

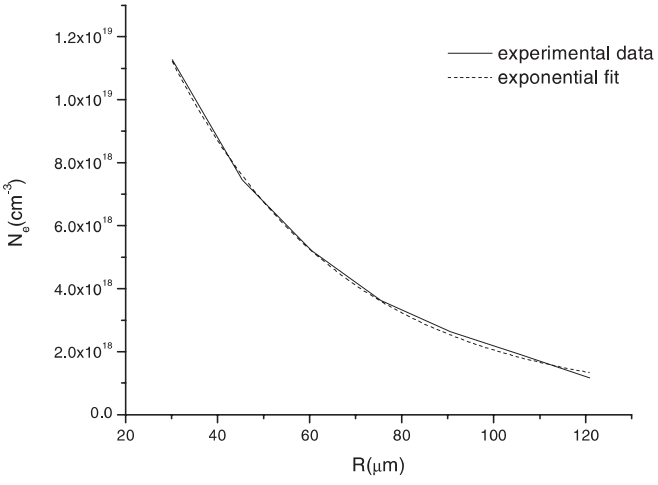


**FIGURE 10** Electron density distribution along the axis of incident laser beam

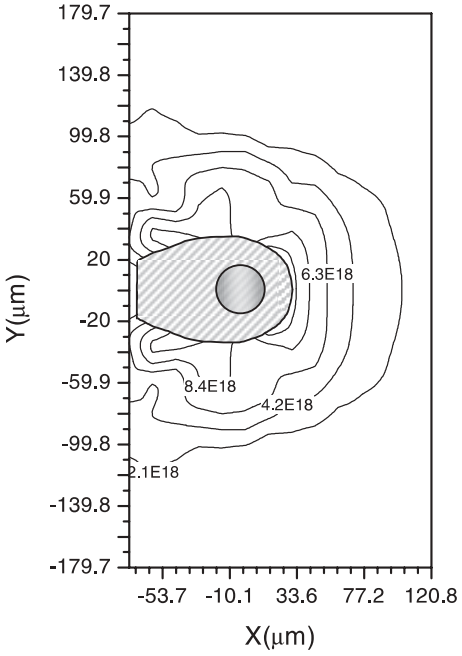


**FIGURE 11** Contour surface plot of electron density ($cm^{-3}$) distribution in droplet plasma

the cross hatched area indicates the approximate position and dimensions of the droplet before irradiation. The Abel inversion in the forward region of laser plasma interaction yields an approximately spherically symmetric electron density distribution. The contour plot also reveals the presence of a jet diagonally behind the droplet.

Comparison of the Medusa and the Abel inversion calculations reveal a discrepancy in the two electron density distributions. This reason for this discrepancy will be investigated in the future and could include some of the following reasons. Unlike our experiment, Medusa assumes uniform irradiation of the target and therefore assumes the laser plasma interaction to be constrained to one dimension; this raises two different sources of error in reference to our experiments. The first is that there may be some recoil or shock to the droplet due to the ejected plasma mass not accounted for in the code. Secondly, due to non-uniform irradiation of the target, some of the deposited laser energy and plasma will be flow laterally instead of radially and therefore decrease the amount of blow off in the direction of the incident laser as compared to the Medusa calculation. Another possible source of error is an early perturbation of the droplet by the low intensity pedestal of the ionizing laser being focused by the front curved surface of the droplet. This could cause early ionization of the rear or inner region of the droplet. Lastly, a shell of water vapor around the evaporating droplet may act to limit the laser energy flow to the body of the droplet, and again decrease the ablation of the droplet.

## 4 Summary

Having a number of favorable qualities, the laser produced water droplet plasma is an effective point source of EUV radiation. Lithium-like oxygen has strong 13 nm line emission well within the band pass of conventional Mo/Si mirrors. The debris emission is minimized by the mass limited target and can be further reduced through the use of an electric repeller field. Application of the 1-D laser-plasma simulation code MEDUSA in conjunction with the synthetic spectra code RATION indicate that there should be strong 13 nm line emission around laser intensities of $4 \times 10^{11}$ W/cm$^2$ in agreement with the recorded spectra. For the first time interferometry has been used to study the laser produced water droplet plasma.

**ACKNOWLEDGEMENTS** This work was supported in part by the State of Florida and by JMAR Research Corp., San Diego. A special note of appreciation is extended to Dr. Greg Shimkaveg of the University of Central Florida, CREOL for useful discussions and technical insight and also to Martin Hipp of Technical University of Graz, Austria for assistance in the use of IDEA.

## REFERENCES

1 F. Jin, K. Gabel, M. Richardson, M. Kado, A.F. Vassiliev, D. Salzmann: Proc. SPIE **2015**, 151 (1993)
2 M. Richardson, K. Gabel, F. Jin, W.T. Silfvast: Proc. OSA Top. Mtg. Soft X-ray Projection Lithography, OSA, Washington DC **18**, 156 (1993)
3 F. Jin, M. Richardson, G. Shimkaveg, D. Torres: Proc. SPIE **2523**, 81 (1995)
4 M. Richardson, D. Torres, C. DePriest, F. Jin, G. Shimkaveg: Opt. Commun. **145**, 109 (1998)
5 L. Rymell, L. Malmqvist, M. Berglund, H.M. Hertz: Microelectron. Eng. **46**, 453 (1999)
6 M. Richardson, W.T. Silfvast, H.A. Bender, A. Hanzo, V.P. Yanovsky, F. Jin, J. Thorpe: Appl. Opt. **32**, 6901 (1993)
7 F. Jin, M. Richardson: Appl. Opt. **34**, No. 25, 5750 (1995)
8 T. Kita, T. Harada, N. Nakano, H. Kuroda: Appl. Opt. **22**, 512 (1983)
9 W. Schwanda, K. Eidmann, M.C. Richardson: J. X-ray Sci. Technol. **4**, 8 (1993)
10 G. Schriever, M. Richardson: To be published (patent pending)
11 P. Rodgers, A. Rogoyski, S. Rose: *MED101: a laser-plasma simulation code. User guide* (Rutherford Appleton Laboratory, 1989)
12 R. Lee: *User Manual for RATION* (University of California and Lawrence Livermore National Laboratory, 1990)
13 R. Benattar, C. Popovics, R. Sigel: Rev. Sci. Instr. **50**(12), 1583 (1979)
14 U. Kogelschatz: Appl. Opt. **13**(8), 1749 (1974)
15 I. Hutchinson: *Principles of Plasma Diagnostics*, (Cambridge University Press, 1992) pp. 112–115
16 http://optics.tu-graz.ac.at/
17 J. Tawney, M. Richardson, R. Adhav: To be published